# Enhanced permafrost warming in European mountains in the early 21st century

Jeannette Noetzli, Ketil Isaksen, Jamie Barnett, Hanne Hvidtfeldt Christiansen, Reynald Delaloye, Bernd Etzelmüller, Daniel Farinotti, Thomas Gallemann, Mauro Gugliemin, Christian Hauck, et al.

# Enhanced permafrost warming in European mountains in the early 21st century

*Jeannette Noetzli*, WSL Institute for Snow and Avalanche Research SLF and Climate Change, Extremes and Natural Hazards in Alpine Regions Research Centre CERC, Davos Dorf, Switzerland*

*Ketil Isaksen, Norwegian Meteorological Institute, Oslo, Norway*

*Jamie Barnett, Department of Geological Sciences, Stockholm University, Stockholm, Sweden*

*Hanne H. Christiansen, Geology Department, University Centre in Svalbard, Longyearbyen, Norway*

*Reynald Delaloye, Department of Geosciences, University of Fribourg, Fribourg, Switzerland*

*Bernd Etzelmueller, Department of Geosciences, University of Oslo, Oslo, Norway*

*Daniel Farinotti, Laboratory of Hydraulics, Hydrology and Glaciology (VAW), ETH Zurich, Switzerland and Swiss Federal Institute for Forest, Snow and Landscape Research WSL, Birmensdorf, Switzerland,*

*Thomas Gallemann, Bavarian Environment Agency, Munich, Germany*

*Mauro Guglielmin, Department of Theoretical and Applied Science, Insubria University, Italy*

*Christian Hauck, Department of Geosciences, University of Fribourg, Fribourg, Switzerland*

*Christin Hilbich, Department of Geosciences, University of Fribourg, Fribourg, Switzerland*

*Martin Hoelzle, Department of Geosciences, University of Fribourg, Fribourg, Switzerland*

*Christophe Lambiel, University of Lausanne, Lausanne, Switzerland*

*Florence Magnin, Laboratoire EDYTEM, CNRS/Université Savoie Mont-Blanc, Le Bourget-du-Lac, France*

*Marc Oliva, University of Barcelona, Barcelona, Spain*

*Paolo Pogliotti, Environmental Protection Agency of Valle d'Aosta, Saint Christophe, Italy*

*Claudia Riedl, GeoSphere Austria, Salzburg, Austria*

*Philippe Schoeneich, PACTE, Institut d'Urbanisme et de Géographie Alpine, Université Grenoble Alpes, France*

*Mauro Valt, Environmental Protection Agency of Veneto, Centro Valanghe di Arabba, Italy*

*Andreas Vieli, Department of Geography, University of Zurich, Zurich, Switzerland*

*Marcia Phillips, WSL Institute for Snow and Avalanche Research SLF and Climate Change, Extremes and Natural Hazards in Alpine Regions Research Centre CERC,, Davos Dorf, Switzerland*

*Corresponding author: Jeannette Noetzli, email: jeannette.noetzli@slf.ch, phone: +41 81 417 0375*

## Abstract

Mountain permafrost, constituting 30% of the global permafrost area, is highly sensitive to climate change and strongly influences mountain ecosystems and communities. This study quantifies 21st century mountain permafrost warming by compiling a quality-controlled permafrost temperature data set obtained in sixty boreholes at monitoring sites in European mountains. Each time series spans one to three decades, enabling a comprehensive assessment of mountain permafrost warming patterns in Europe, from the Alps, across Scandinavia to Svalbard in the high Arctic. We find consistent permafrost warming patterns across, all observed sites, depths and time periods. For the early 21st century, warming rates at 10 and 20 meters depth exceeded 1 °C per decade in cases, and are generally higher than previously reported as a result of both, accelerated warming and a more comprehensive data set. Substantial warming notably occurs at cold and ice-poor bedrock sites at both high latitudes and high elevations, with the permafrost warming rates being comparable to warming rates of air temperature.

For ice-rich sites close to the melting point instead, latent heat effects reduce temperature changes, thus obscuring important changes ongoing in ice-rich permafrost substrates.

## 1. Introduction

While the 21st century retreat of glaciers has garnered significant attention [1,2], permafrost worldwide has undergone widespread and persistent but less visible changes [3–12]. Permafrost is a key component of the cryosphere and is recognized as an Essential Climate Variable of the Global Climate Observation System [13]. It is defined on a thermal and temporal basis as ground with a maximum temperature of 0 °C for at least two consecutive years. Mountain permafrost, constituting 30% of the global permafrost area [14,15], spans low to high latitudes in both hemispheres and all continents. Complex mountain topography leads to a high spatial variability and large environmental gradients in these areas, thus controlling the permafrost distribution [e.g., 16,17]. Mountain permafrost is highly sensitive to the pronounced atmospheric warming observed at high elevations [18]. This warming and degradation of permafrost has implications for the stability of steep, perennially frozen mountain slopes [19–25] with potential impacts and risks to both human safety [26–28] and infrastructure [29], as well as effects on ecosystems [30–33] or hydrological processes [34–36].

The monitoring and assessment of permafrost changes in polar and high-mountain regions relies on long-term records of ground temperatures measured in boreholes [37–39]. Near surface ground temperatures fluctuate in response to changes in atmospheric conditions. These variations are increasingly attenuated and delayed with depth. At the so-called Depth of Zero Annual Amplitude (DZAA), seasonal temperature changes become negligible and their variations follow long-term climate-related changes. For the period 2007–2016, Biskaborn et al. [3] reported global permafrost warming at the DZAA of 0.29 °C $dec^{-1}$ and of 0.19 °C $dec^{-1}$ for mountain regions. The 40 mountain permafrost sites included in that study (of which about half were in Europe) were considered in a lumped manner, i.e. without accounting for the high variability in topographic and ground ice conditions and, consequently, in the rates of permafrost warming. Regional or local studies on changes in mountain permafrost point to these differences [7–9,11,40–42]. However, they are typically restricted to single sites or regions, and are not directly comparable due to differences in the considered time periods, observation methods, or recording depths.

Systematic research on permafrost in mountain regions began in the late 1970s [e.g., 43–45,for a review see 46] driven by tourism and infrastructure development in the European mountains, where the most densely populated permafrost landscapes are found. The growing demand for knowledge about permafrost distribution and related processes prompted the rapid development of research in that environment. The 60 m deep borehole drilled in 1987 at Murtèl-Corvatsch rock glacier, Swiss Alps, provides the longest time series of permafrost temperatures in Europe [47,48]. Climate-related permafrost monitoring in the European mountains was initiated in the late 1990s, with a borehole transect from High-Arctic Svalbard to the Mediterranean Sierra Nevada Mountains (PACE, Permafrost and Climate in Europe) [7,49].

Although several national and regional permafrost observation programs have been established since then [50–56] and although activities in the framework of the Global Terrestrial Network for Permafrost increased [37], there is no Europe-wide coordination of permafrost data to date. Many time series are thus held by regional offices or individual researchers.

For an extended and consistent analysis of permafrost warming pattern across European mountains, we compiled a distinct data set of 60 temperature time series measured in boreholes in or next to permafrost area. The data set covers sites representing typical landforms found in mountain permafrost from the Sierra Nevada and Alps to Scandinavia and high Arctic Svalbard (Fig. 1) and includes time series that cover at least one decade and that reach a depth of 10 m or more. Data are consistently aggregated to mean annual ground temperatures (MAGT), which are then used to derive temperature change rates for decadal or 20-year periods. To assess the spatial and temporal variability of warming patterns, we consider running mean temperature change rates, as well as a classification by depth ranges, permafrost conditions, ground ice content, and surface cover. We find evidence for permafrost warming across all European mountain regions, depths, time spans and periods considered. Differences in the observed warming patterns depend primarily on the amount of exchanged latent heat, which can significantly reduce temperature change rates in frozen ground due to phase change, as well as on the depth range. Warming rates are highest in the uppermost 10 meters, at cold permafrost sites, and at sites with low ground ice content (i.e. in bedrock) where effects of latent heat are largely absent. Here, warming rates are comparable or higher in their magnitude to non-permafrost ground or surface air temperature (SAT). With increasing ground ice content and ground temperatures towards 0°C, warming rates decrease to very small values. For these sites, temperature measurements do not reveal the ongoing changes. The observed patterns prove robust across all depths, time spans and periods considered, surpassing regional differences in prominence.

Permafrost warming is a relatively slow yet inexorable process. The higher warming observed in the upper decameter of the ground, points to a significant increase in thermal disequilibrium. The future propagation of these changes to greater depths is largely predetermined already. Our study underlines the significance of maintaining uninterrupted long records of permafrost temperatures for the assessment of climate change impacts. Further efforts to ensure the systematic and sustained acquisition, curation and public dissemination of long-term permafrost records need thus to be endorsed at both national and international levels.

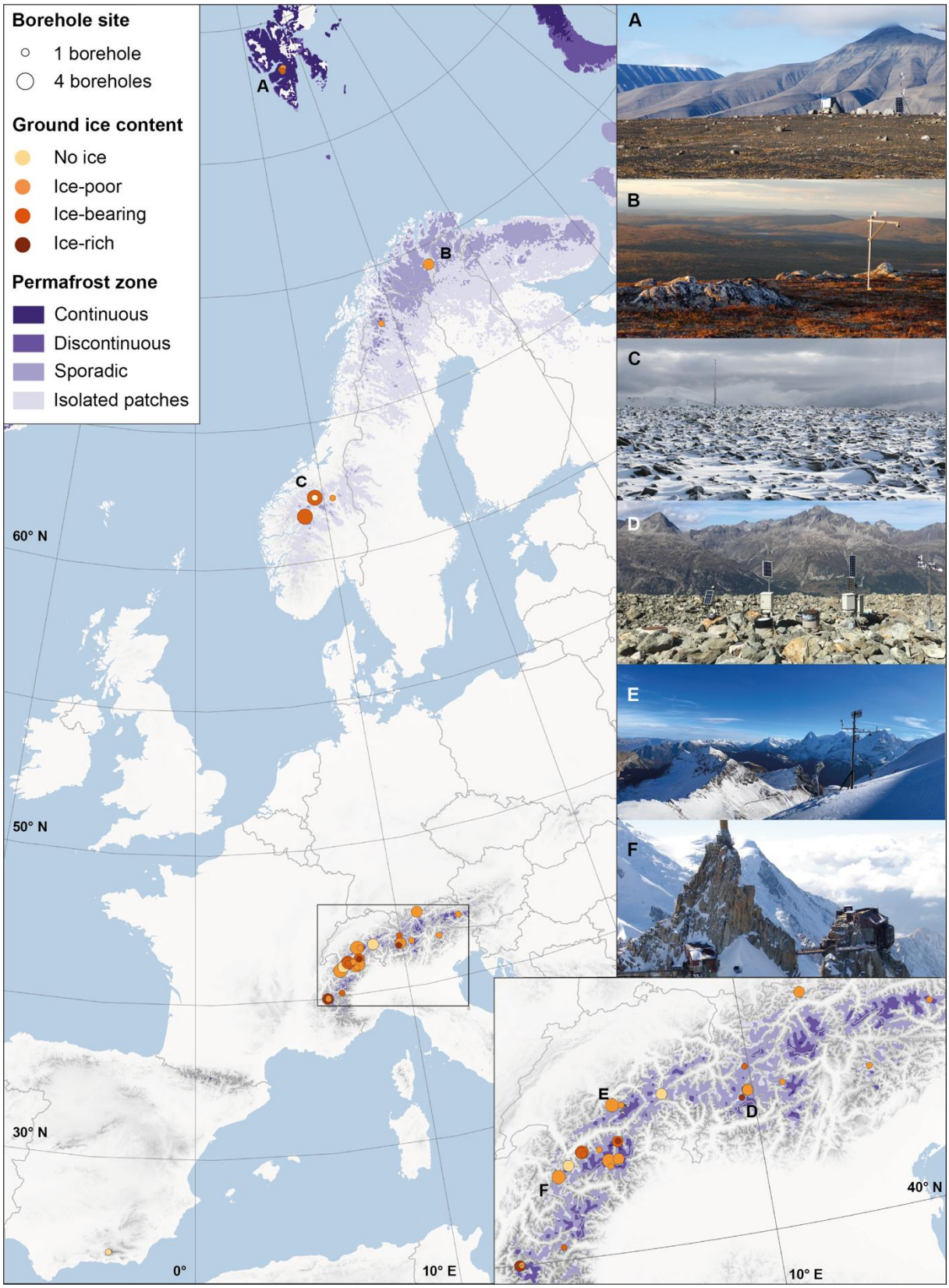


*Figure 1. Overview of the location of the borehole sites in European mountain regions where long permafrost temperature time series are obtained from Svalbard to the Sierra Nevada. A zoom on the Alpine Arc is given at the lower right. Each site is shown as one point with the size indicating the number of boreholes. The color indicates the general ground ice content (cf. Table 1). To the right, impressions of several sites are shown to highlight the variable characteristics. Data sources: the permafrost zones are based on Obu et al (2019) [15], background topography is from the GMTED2010, country outlines are*

*taken from Eurostat (@EuroGraphics and UN-FAO), glacier outlines for Svalbard are from GLIMS and NSIDC (2018). Photos show the sites Janssonhaugen (A), Iskoras (B), Dovrefjell (C), Murtél-Corvatsch (D), Schilthorn (E), and Aiguille du Midi (F) and were taken by K. Isaksen (A–C), J. Noetzli (D), A. Hasler (E), and S. Gruber (F).*

## 2. Results

### 2.1 Measured permafrost temperatures in European mountains

The data set used in this study includes 60 ground temperature time series measured in boreholes in mountain permafrost regions in Europe, i.e. Sierra Nevada, the Alps, Scandinavia as well as Svalbard (cf. Supplementary material, Figs. S1 and S2, Table 1). Data from other European mountain regions, such as the Pyrenees or Greenland, were not accessible. The collected data are measured at 35 sites between 37 and 78° N and at elevations between 275 and 3800 m asl. in 8 countries (Fig. 1). Two boreholes are situated on Svalbard, 13 in Scandinavia (NO, SE), 15 in the Central and Eastern Alps (CH, IT, DE, AT), 29 in the Western Alps (FR, IT, CH) and one in the Sierra Nevada (SP). Sites are located in typical landforms found in mountain permafrost such as talus or bedrock slopes, crests or plateau blockfields, in rock glaciers, or moraines. The longest time series, started in 1988, covers 35 years and is measured in rock glacier Murtèl-Corvatsch/CH. Four time series from the Western and Central Alps just cover a decade (Fig. 2).

Permafrost temperatures recorded in European mountains range from cold permafrost, with MAGT at 10 m depth as low as –6.2 °C for sites at the highest elevations and latitudes, to degrading permafrost, with temperatures at or just below 0 °C (Fig. 2). Cold permafrost with MAGT below –4 °C is found at elevated places in Svalbard (Breinosa, Janssonhaugen) as well as in North-facing bedrock slopes at elevations above 3500 m asl. in the Western Alps (Jungfrau Ridge, Aiguille du Midi). Surface MAGTs of less than –12 °C have been measured on northern slopes in the Western Alps at elevations well above 4000 m asl. (Pogliotti et al. 2023). However, long-term observations at depth from such locations are not available to date. Degrading permafrost with temperatures close to 0 °C is found in all parts of the Alps as well as on the Scandinavian mainland, mainly in ice-bearing talus slopes at elevations around 2500 m asl. or in blockfields (for example at Bellecombes, Gentianes, Les Attelas, Schilthorn, Schafberg, Dovrefjell, Tron, Iskoras). Permafrost temperatures in the Central and Eastern Alps do not reach as low as in the Western Alps, which is due to the lower mountains in these regions and the lack of observations > 3000 m asl. rather than to climatic differences. Eight of the sixty borehole time series (13%) are not measured in but just next to permafrost for their entire profile and observation period (all MAGT >0 °C). At these non-permafrost sites, MAGT range up to >3 °C (Veleta Peak in the Sierra Nevada/SP and south-exposed bedrock ridge at Gemsstock/CH).

41 of the 53 time series (77%) with available MAGT data at 10 m depth for one of the past three years (2020–2022) reached their maximum value in these three years (Fig. 2). Similarly, 26 time series out of 35 (74%) reached their maximum at 20 m depth in one of the same years. However, the two sites on

Svalbard (the coldest time series in Fig. 2a) experienced their maximum before 2020 due to the extremely warm years 2016–2018. MAGT at 10 m depth increased to above 0 °C during the measurement period for 9 borehole time series (17%).

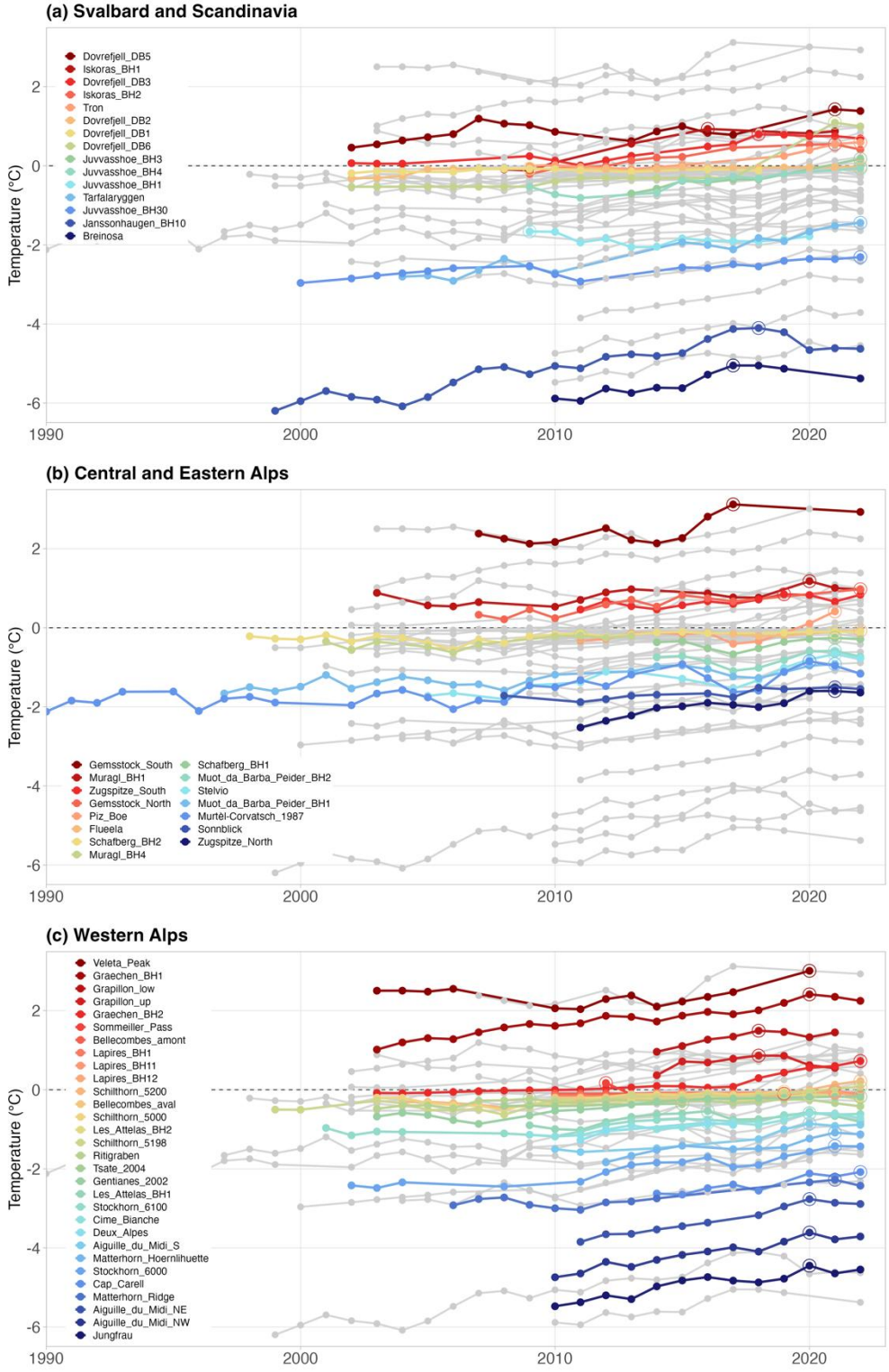


*Figure 2. Sixty records of mean annual ground temperatures (MAGT) obtained in European mountain permafrost at approximately 10 m depth and covering at least one decade: Svalbard and Scandinavia (a, sites in Spitsbergen on Svalbard, mainland Norway, and Sweden), Central and Eastern Alps (b, sites in Central and Eastern Switzerland, North-eastern Italy, Germany and Austria), and Western Alps (b, sites in France, Western Switzerland and North-western Italy and including the*

*site in the Spanish Sierra Nevada). All available time series are shown in grey for comparison. The circles indicate the maximum MAGT of each time series.*

## 2.2 Permafrost warming rates

Temperature change rates at 10 m depth for the period 2013–2022 (or for the latest decade with data available ending in the past 5 years for 9 boreholes) range from –0.10 to 1.77 °C dec$^{-1}$ (Table 1, n=55). The mean warming rate for sites where permafrost is present at this depth for all or part of the decade is 0.42 °C dec$^{-1}$ (n=47, median 0.39 °C dec$^{-1}$) with a standard error of 0.05 °C dec$^{-1}$. For 45% of the permafrost time series, the warming rate is larger than 0.5 °C dec$^{-1}$. Highest warming rates above 0.7 °C dec$^{-1}$ are typically measured in bedrock slopes and where permafrost is cold or absent. Also, in debris slopes where permafrost has degraded during the ten-year period, warming rates can be high: the highest warming rate of 1.77 °C dec$^{-1}$ was observed for Dovrefjell DB6 in southern Norway. Warming rates smaller than 0.5 °C are typically observed in ice-bearing talus slopes and blockfields or in rock glaciers. Cooling rates were obtained for 4 locations in ice-bearing talus slopes or blockfields. Cooling rates are, however, smaller than 0.1 °C dec$^{-1}$ at 10 m and smaller than 0.2 °C dec$^{-1}$ at 20 m depth.

At lower depth and for a longer time period, permafrost warming rates are lower: they range up to 0.71 °C dec$^{-1}$ for 2013–2022 at 20 m depth (mean 0.24 °C dec$^{-1}$ ; n=33) and up to 0.85 °C dec$^{-1}$ for 2003–2022 at 10 m depth (mean 0.39 °C dec$^{-1}$ ; n=16). This shows a delayed propagation of the recent warming to greater depths, related to slow heat conduction processes. For the time period 2007–2016, the global-scale analysis by Biskaborn et al. [3] found an average warming rate of 0.19 °C dec$^{-1}$ at the DZAA, while we obtain a mean warming rate of 0.42 °C dec$^{-1}$ at a depth of 10 m (n=22) and of 0.24 °C dec$^{-1}$ at 20 m depth (n=20). Calculating the warming rate for the same group of time series and the period 2013–2022, results in 0.43 and 0.26 °C dec$^{-1}$ for 10 and 20 m depth, respectively.

*Table 1. Boreholes in European mountains in or close to permafrost area together with key meta information and calculated 2013–2022 decadal warming rates at 10 m depth. If the time series did not extend to 2022, the latest available decadal period (ending no later than 2018) was considered (*). The number (n) of mean annual ground temperature (MAGT) values available to compute the warming rate is given together with a coefficient of determination ($R^2$). The color coding helps in discerning the magnitude of the warming rate. "Start" relates to the first year of the time series, "Dep" denotes the total depth of the borehole, "Lat" the latitude and "Ele" the elevation. MGT is the mean ground temperature of the latest decade (with minimum and maximum MAGT in brackets). Five of the boreholes shown in Figs. 1 and 2 are not included as no recent decadal warming rate could be calculated at 10 m.*

| Borehole(Country) | Start | Dep. (m) | Lat. (°) | Elev. (m) | Ground ice cont. | Surface cover | MGT (min/max MAGT) (°C) | Permafrost (10 m) | Warming rate (°C dec$^{-1}$) (n/$R^2$) |
|---|---|---|---|---|---|---|---|---|---|
| Aiguille du Midi NE (FR) | 2011 | 10 | 45.877 | 3745 | ice-poor | bedrock | –3.2 (–3.6/–2.8) | cold | 0.98 (9/0.93) |
| Aiguille du Midi NW (FR) | 2010 | 10 | 45.880 | 3738 | ice-poor | bedrock | –4 (–4.5/–3.6) | cold | 0.85 (10/0.88) |
| Aiguille du Midi S (FR) | 2010 | 10 | 45.880 | 3753 | ice-poor | bedrock | –1.1 (–1.5/–0.9) | warm | 0.82 (6/0.89) |
| Bellecombes amont (FR) | 2010 | 14 | 44.995 | 2725 | ice-rich | debris | –0.1 (–0.1/–0.1)* | deg | 0.00 (8/0.53) |
| Bellecombes aval (FR) | 2010 | 14 | 44.995 | 2710 | ice-rich | debris | –0.2 (–0.3/–0.2)* | deg | –0.07 (6/0.78) |
| Breinosa (NO) | 2010 | 334 | 78.142 | 677 | ice-bearing | blockfield | –5.4 (–5.7/–5.0) | cold | 0.58 (8/0.37) |
| Capanna Carell (IT) | 2014 | 10 | 45.973 | 3800 | ice-poor | bedrock | –2.4 (–2.7/-2.1) | cold | 0.73 (8/0.85) |
| Cime Bianche (IT) | 2008 | 41 | 45.919 | 3100 | ice-poor | bedrock | –0.8 (–1.0/–0.6) | warm | 0.39 (10/0.73) |
| Dovrefjell DB1 (NO) | 2002 | 7 | 62.297 | 1505 | ice-bearing | debris | –0.1 (–0.2/–0.1)* | deg | –0.01 (5/0.03) |
| Dovrefjell DB2 (NO) | 2003 | 9 | 62.296 | 1481 | ice-bearing | debris | –0.1 (–0.1/0) | deg | 0.08 (10/0.54) |

| | | | | | | | | | |
|---|---|---|---|---|---|---|---|---|---|
| *Dovrefjell DB3 (NO)* | 2002 | 9 | 62.296 | 1477 | no ice | debris | 0.6 (0.3/0.8) | no | 0.55 (8/0.70) |
| *Dovrefjell DB5 (NO)* | 2002 | 9 | 62.300 | 1458 | no ice | debris | 1.0 (0.6/1.4) | no | 0.80 (7/0.81) |
| *Dovrefjell DB6 (NO)* | 2002 | 9 | 62.293 | 1402 | ice-bearing | debris | 0.1 (–0.3/1.1) | no | 1.77 (7/0.84) |
| *Gemsstock N (CH)* | 2007 | 20 | 46.601 | 2905 | no ice | bedrock | 0.7 (0.5/1.0) | no | 0.34 (6/0.55) |
| *Gemsstock S (CH)* | 2007 | 20 | 46.601 | 2905 | no ice | bedrock | 2.6 (2.1/3.1) | no | 0.97 (6/0.53) |
| *Gentianes 2002 (CH)* | 2003 | 20 | 46.084 | 2888 | ice-bearing | debris | –0.2 (–0.4/–0.2) | deg | 0.19 (10/0.83) |
| *Graechen BH1 (CH)* | 2003 | 24 | 46.171 | 2450 | ice-bearing | debris | 2.1 (1.7/2.4) | no | 0.70 (10/0.82) |
| *Graechen BH2 (CH)* | 2003 | 24 | 46.171 | 2450 | ice-bearing | debris | 0.3 (0.1/0.7) | no | 0.80 (10/0.87) |
| *Grapillon low (IT)* | 2013 | 20 | 45.909 | 3100 | no ice | bedrock | 1.3 (1.0/1.5) | no | 0.63 (8/0.68) |
| *Grapillon up (IT)* | 2013 | 20 | 45.909 | 3100 | no ice | bedrock | 0.7 (0.4/0.9) | no | 0.17 (8/0.06) |
| *Iskoras BH1 (NO)* | 2008 | 10 | 69.302 | 585 | ice-poor | bedrock | 0.6 (0.1/0.9)* | no | 0.75 (5/0.72) |
| *Iskoras BH2 (NO)* | 2009 | 57 | 69.301 | 591 | ice-poor | debris | 0.4 (0.1/0.5) | no | 0.41 (7/0.75) |
| *Janssonhaugen BH10 (NO)* | 1998 | 100 | 78.183 | 275 | ice-poor | bedrock | –4.5 (–4.8/–4.1) | cold | 0.22 (10/0.06) |
| *Jungfrau (CH)* | 2010 | 17 | 46.546 | 3590 | ice-poor | bedrock | –4.8 (–5.3/–4.4) | cold | 0.65 (10/0.7) |
| *Juvvasshoe BH1 (NO)* | 2009 | 10 | 61.676 | 1851 | ice-bearing | blockfield | –1.9 (–2.1/–1.8)* | warm | 0.17 (9/0.25) |
| *Juvvasshoe BH3 (NO)* | 2009 | 10 | 61.697 | 1561 | ice-poor | debris | –0.4 (–0.7/0.2) | no | 0.89 (7/0.93) |
| *Juvvasshoe BH30 (NO)* | 2000 | 100 | 61.683 | 1894 | ice-poor | blockfield | –2.5 (–2.9/–2.4)* | cold | 0.56 (9/0.92) |
| *Juvvasshoe BH4 (NO)* | 2009 | 14 | 61.700 | 1547 | ice-poor | bedrock | –0.3 (–0.7/–0.1) | deg | 0.64 (7/0.81) |
| *Lapires BH1 (CH)* | 2000 | 19.6 | 46.106 | 2500 | ice-bearing | debris | –0.1 (–0.1/–0.1) | deg | 0.02 (10/0.25) |
| *Lapires BH11 (CH)* | 2009 | 40 | 46.106 | 2500 | ice-bearing | debris | –0.1 (–0.3/0) | deg | 0.17 (7/0.61) |
| *Lapires BH12 (CH)* | 2010 | 35 | 46.106 | 2535 | ice-bearing | debris | –0.1 (–0.3/–0.1) | deg | 0.10 (10/0.25) |
| *Les Attelas BH1 (CH)* | 2009 | 26 | 46.097 | 2661 | ice-bearing | debris | –0.7 (-0.8/–0.5) | warm | –0.10 (10/0.11) |
| *Les Attelas BH2 (CH)* | 2008 | 21 | 46.097 | 2689 | ice-bearing | debris | –0.2 (-0.3/–0.1) | deg | 0.05 (8/0.06) |
| *Matterhorn Hoernlih. (CH)* | 2012 | 60 | 45.982 | 3295 | ice-poor | bedrock | –1.4 (–1.7/–1.1) | warm | 0.54 (9/0.76) |
| *Matterhorn Ridge (CH)* | 2006 | 60 | 45.982 | 3295 | ice-poor | bedrock | –2.5 (–2.8/–2.3) | cold | 0.56 (5/0.89) |
| *Muot d. Barba P. BH1 (CH)* | 1997 | 18 | 46.496 | 2946 | ice-poor | debris | –1.1 (–1.3/–0.9) | warm | 0.04 (9/0.01) |
| *Muot d. Barba P. BH2 (CH)* | 1997 | 38 | 46.497 | 2942 | ice-poor | debris | –0.8 (–1.1/–0.6) | warm | 0.20 (9/0.10) |
| *Muragl BH1 (CH)* | 2002 | 60 | 46.508 | 2549 | no ice | coarse bl. | 0.9 (0.8/1.2) | no | 0.16 (7/0.11) |
| *Murtèl-Corvatsch 87(CH)* | 1988 | 62 | 46.429 | 2670 | ice-rich | coarse bl. | –1.2 (–1.6/–0.8) | warm | 0.19 (9/0.04) |
| *Piz Boe (IT)* | 2011 | 30 | 46.510 | 2900 | ice-poor | bedrock | –0.1 (–0.4/0.4) | no | 0.46 (9/0.27) |
| *Ritigraben (CH)* | 2002 | 13 | 46.175 | 2634 | ice-rich | coarse bl. | –0.3 (–0.4/–0.2) | deg | –0.09 (11/0.27) |
| *Schafberg BH1 (CH)* | 2014 | 16 | 46.497 | 2754 | ice-rich | coarse bl. | –0.4 (–0.7/–0.3) | deg | 0.22 (9/0.19) |
| *Schafberg BH2 (CH)* | 1997 | 60 | 46.499 | 2732 | ice-rich | coarse bl. | –0.1 (–0.2/–0.1) | deg | 0.05 (8/0.45) |
| *Schilthorn 5000 (CH)* | 2002 | 100 | 46.558 | 2909 | ice-poor | debris | –0.1 (–0.4/–0.1)* | degr | 0.25 (9/0.74) |
| *Schilthorn 5198 (CH)* | 1999 | 14 | 46.558 | 2910 | ice-poor | debris | –0.1 (–0.2/0.1) | no | 0.26 (10/0.71) |
| *Schilthorn 5200 (CH)* | 2003 | 100 | 46.558 | 2909 | ice-poor | debris | –0.1 (–0.3/0.2) | no | 0.51 (10/0.89) |
| *Sonnblick (AT)* | 2008 | 20 | 47.054 | 3106 | ice-poor | bedrock | –1.6 (–1.8/–1.5) | warm | 0.24 (8/0.60) |
| *Stelvio (IT)* | 1999 | 100 | 46.516 | 3000 | ice-poor | bedrock | –1.1 (–1.5/–0.7) | warm | 0.67 (8/0.43) |
| *Stockhorn 6000 (CH)* | 2001 | 100 | 45.987 | 3412 | ice-poor | bedrock | –1.7 (–2/–1.4) | warm | 0.52 (10/0.65) |
| *Stockhorn 6100 (CH)* | 2001 | 17 | 45.987 | 3410 | ice-poor | bedrock | –0.7 (–0.8/–0.6) | warm | 0.22 (10/0.63) |
| *Tarfalaryggen (SE)* | 2000 | 100 | 67.917 | 1550 | ice-poor | bedrock | –2.0 (–2.7/–1.7)* | cold | 0.93 (8/0.85) |
| *Tron (NO)* | 2008 | 29 | 62.174 | 1640 | ice-poor | blockfield | 0.2 (–0.1/0.6) | no | 0.76 (7/0.97) |
| *Veleta Peak (SP)* | 2002 | 100 | 37.056 | 3380 | no ice | bedrock | 2.4 (2.1/3.0) | no | 0.87 (7/0.65) |
| *Zugspitze N (DE)* | 2010 | 20 | 47.422 | 2922 | ice-poor | bedrock | –1.9 (–2.2/–1.6) | warm | 0.61 (10/0.79) |
| *Zugspitze S (DE)* | 2010 | 20 | 47.422 | 2922 | ice-poor | bedrock | 0.7 (0.5/0.8)* | no | 0.36 (10/0.67) |

Warming rates vary between time periods, depending on the inter-annual variability of the MAGT (which is related to the depth). This variability is shown by computing warming rates over a moving window of 10 or 20 years (Fig. 3). The fast reaction of temperatures in the uppermost metres (i.e. at 5 m depth) to inter-annual variations in air temperature and snow conditions, leads to a high variability of decadal warming rates: they can fluctuate by more than 1.5 °C dec$^{-1}$ when moving the averaging window by only 5 years. Due to this high variability, decadal warming rates at 5 m depths are not suited to describe long-term changes in permafrost. Warming rates for greater depths of 10 and 20 m exhibit lower variation but can still vary up to nearly 1 and 0.5 °C dec$^{-1}$, respectively. Considering 20y periods, the variability is significantly lower than for decadal warming rates, and rates at 5 m depth are similar

to 10 m depth. Figure 4 shows the variability of decadal warming rates at 10 m depth for all boreholes. The length of the time series also influences this variability. The most recent values (diamonds in Fig. 4) are at the upper end of the observations for most boreholes. However, at the coldest sites and for some sites in Svalbard (e.g. Breinosa/NO, Janssonhaugen/NO, Aiguille du Midi/FR), most recent decadal warming rates are lower than those obtained with earlier data.

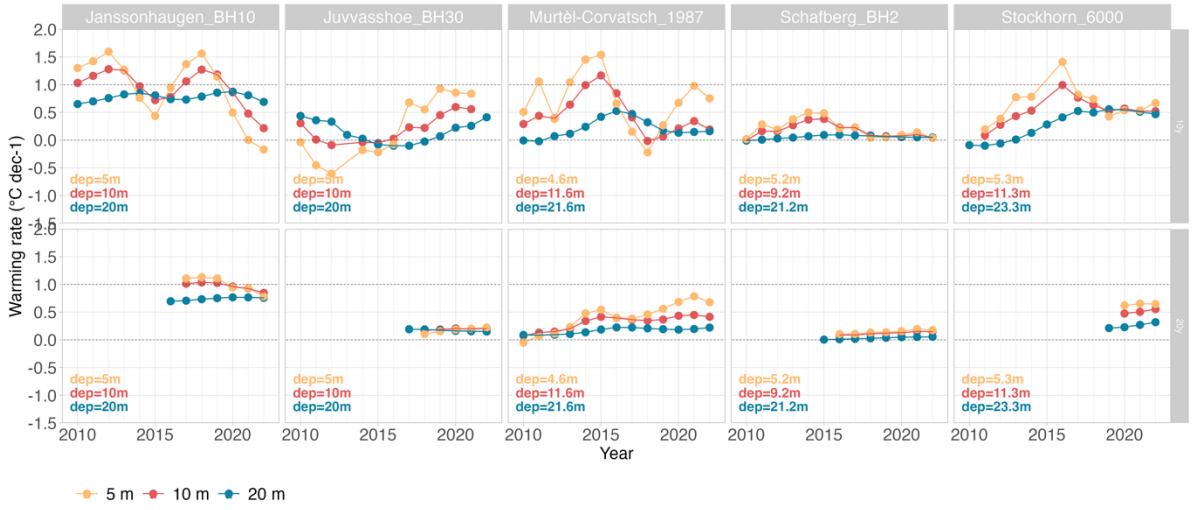


*Figure 3. Examples of running warming rates for permafrost temperature time series with an averaging window of one (top) and two (bottom) decades. Depths of 5, 10 and 20 m are distinguished by colours. Values are plotted at the end of the period, e.g. the warming rates for 2013–2022 are shown at x=2022. Actual depths of the sensors are indicated at the bottom of each plot.*

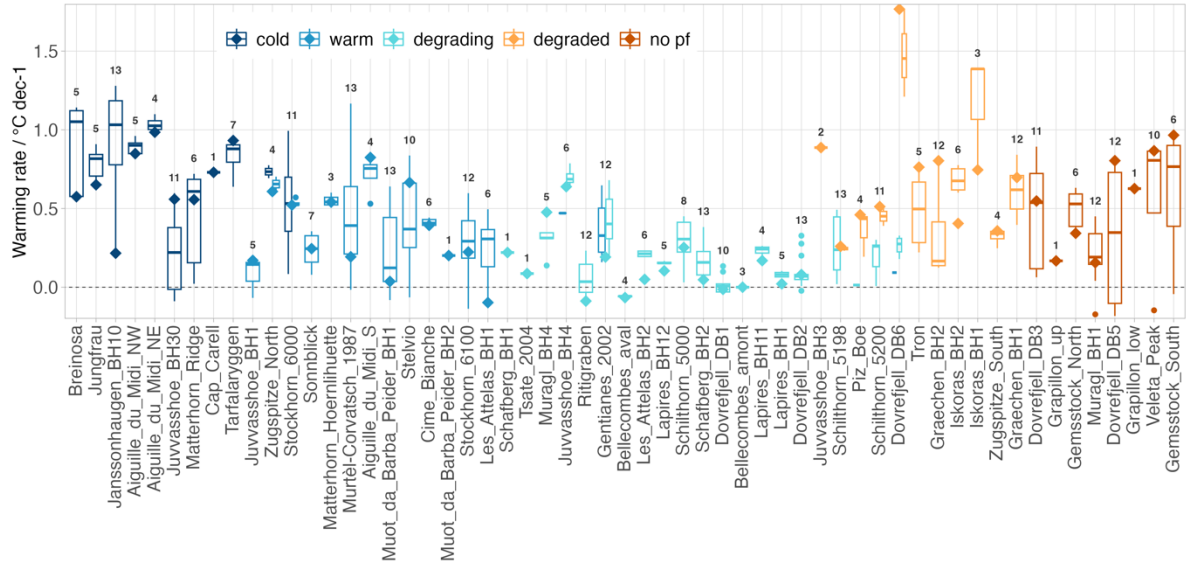


*Figure 4. Boxplots of permafrost warming rates at 10 m depth obtained from ground temperature measurements in the European mountains for all available 10 year periods starting from 2000. Diamonds show the warming rate for the latest available decade (2013–2022 or max. 4 years earlier, cf. Table 1). The number of values per borehole is indicated on top of the boxes. Boreholes are sorted by their mean ground temperature (MGT) during the last decade, with the coldest to the left.*

*The colours indicate the permafrost conditions («cold» means «no_pf» indicates the eight non-permafrost boreholes and «degraded» includes boreholes that were in permafrost at the beginning but not at the end of the latest decade).*

## 2.3 Permafrost warming patterns

We observe a general decrease in warming rates with ground temperatures increasing towards 0 °C (Figs. 4 and 5). In ice-rich ground like rock glaciers, ground temperatures can remain just below 0 °C for many years, i.e. until all ground ice has melted (e.g., Ritigraben/CH, Schafberg/CH, Bellecombes/FR). In our dataset, ice-rich and ice-bearing sites are in warm or degrading permafrost (MGT>–2 °C) and corresponding decadal warming rates are below 0.3 °C dec$^{-1}$ at 10 m depth (Fig. 5), with the exception of the cold site Breinosa/NO. The same pattern is also observed for 20 m depth and 20-year time periods, although with less data points. Once the ground ice has melted, warming rates significantly increase as the buffering effect of latent heat is no longer effective (cf. originally ice-containing sites with MGT > 0 °C in Fig. 5 and degraded sites in Fig. 4). Sites that are next to but not in permafrost have warming rates comparable to those in cold permafrost (Figs. 4 and 5).

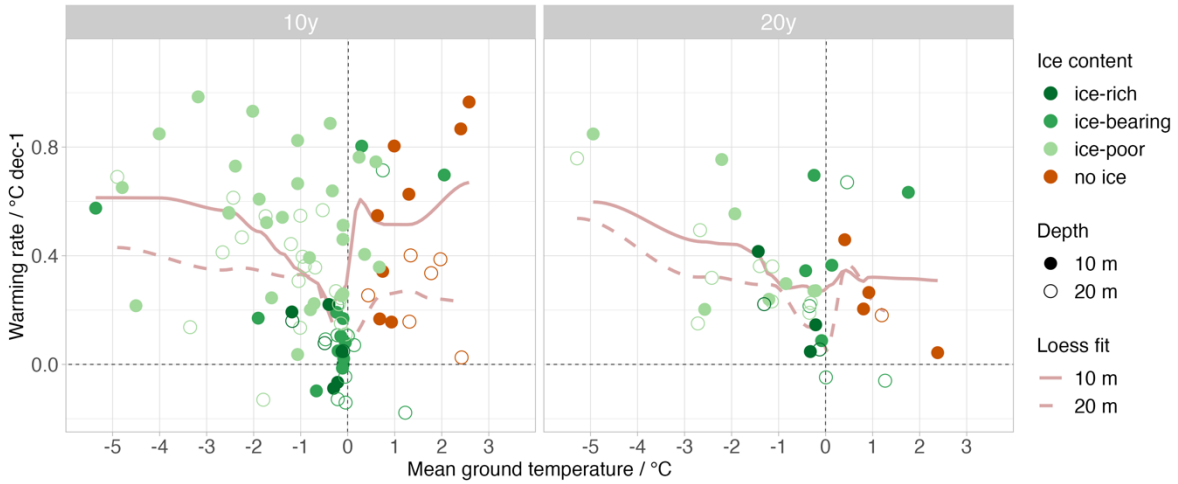


*Figure 5. Warming rates of ground temperatures at 10 and 20 m depth for the periods 2013–2022 (10y, left) and 2003–2022 (20y, right) plotted against the mean ground temperature (MGT) during the same period. The light red lines show a non-parametric fit (zero degree loess fit with span=0.4) to illustrate the relation between the two quantities at 10 m (solid) and 20 m depth (dashed). The highest decadal warming rate at 10 m depth (1.77 °C dec–1) lies outside the plot area but is considered for the loess fit. Points with no ground ice («no ice») are boreholes outside permafrost conditions. Green points with positive MGT originally were in permafrost but have degraded during the period considered.*

Mean warming rates of permafrost at 10 m depth for the latest available decade are 0.36 °C dec$^{-1}$ in the European Alps (n=34), 0.4 °C dec$^{-1}$ for Svalbard (n=2) and 0.63 °C dec$^{-1}$ for Scandinavia (n=11). Differences related to the thermal conditions, i.e. to permafrost classes, surpass these regional differences (Fig. 6): cold permafrost for the same period and depth warms at a mean rate of 0.67 °C dec$^{-1}$ (n=9), compared to 0.35 °C dec$^{-1}$ for warm permafrost (n=13) and 0.11 °C dec$^{-1}$ for degrading permafrost (n=14). Ground temperatures at sites where permafrost has degraded during the considered

time period (n=11) or is absent (n=8), are increasing by 0.64 °C dec$^{-1}$ on average (n=19). The classification by ground ice content (cf. section 4.2) confirms this picture: for ice-rich rock glaciers, warming rates at a depth of 10 m are very low (0.05 °C dec$^{-1}$, n=6). For ice-bearing sites like talus slopes or moraines, they are 0.35 °C dec$^{-1}$, n=13), whilst sites with only little to no ground ice warm at decadal rates of 0.5–0.6 °C dec$^{-1}$. Characteristics of the surface cover are typically related to the type of landform and, therefore, again to the ground ice content. Warming rates in cold permafrost, at ice-poor bedrock sites and at non-permafrost sites are in a similar range, corresponding to SAT warming rates over the past 30 years (cf. section 4.3 for details on the calculation). These patterns, referring to the latest decade and a depth of 10 m, prove consistent across all considered depths, time periods and time spans (cf. supplementary material, Figs. S6–S9).

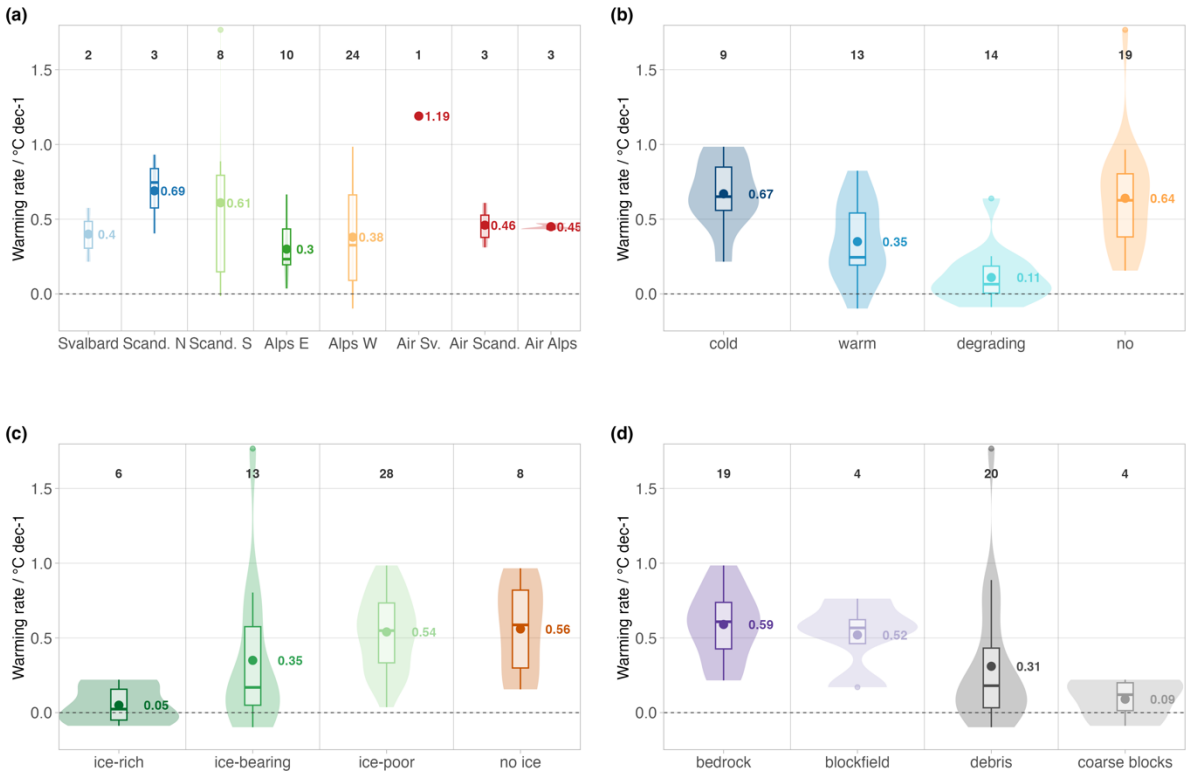


*Figure 6. Permafrost warming rates at a depth of 10 m for the latest available decade (2013–2022 or <5 years earlier), classified by (a) region, (b) permafrost class, (c) ground ice content, and (d) surface cover. The distribution of individual warming rates per class is shown by the violins and overlaying boxplots, the mean values are shown by filled dots and in °C dec$^{-1}$next to it. The number of time series included in each class are given by black numbers at the top. The eight boreholes outside of permafrost (labelled "no ice") are not included in (a) and (d) and are part of the class "degrading" in (b). Zero warming is highlighted by the dashed horizontal line. Warming rates of air temperatures at high-elevation stations for the 30-year period 1993–2022 are shown for comparison in (a) (data source: MeteoSwiss, METNorway, UNIS).*

## 2.4 Seasonal distribution of warming

Examination of monthly ground temperatures at 10 m depth reveals distinct differences in warming rates over the course of the year, characterized by prominent months for both the highest and lowest values,

and showing a typical spread of 0.2–0.4 °C dec$^{-1}$ (Fig. 7). With regard to the categorized permafrost condition, surface type and ground ice content, the patterns observed for the monthly warming rates are consistent with the annual values (Fig. 6). Notable differences emerge between the most recent decade 2013–2022 and the 20-year period from 2003–2022 (Fig. 7, left). On average, the maximum monthly warming rate in cold permafrost was 0.75 °C dec$^{-1}$. The highest monthly values in cold permafrost for the 10-year and 20-year periods were observed at Aiguille du Midi NE in the Western Alps (warming rate of 1.1 °C dec$^{-1}$ occurring at 10 m depth in November, with a phase lag of five months with respect to the ground surface) and at Janssonhaugen BH10 in Svalbard (0.9 °C dec$^{-1}$ occurring in June at 10 m depth, with a phase lag of seven months with respect to the ground surface).

For the latest decade, the highest monthly warming rates at 10 m depth originate from increased near ground surface temperatures in summer and autumn, while for the 20-year period, the highest monthly warming rates at 10 m are predominantly influenced by the warming occurring near the ground surface during winter (Figure 7, right). However, the manner in which the highest warming rates are distributed in summer and autumn differs across permafrost classes. In the case of cold and warm permafrost, the warming is equally distributed between summer and autumn. For degrading permafrost, autumn has a significantly higher influence in terms of warming compared to summer. In areas without permafrost, summer clearly emerges as the dominant warming season. For the 20-year period, instead, winter stands out as the dominant warming season across all permafrost classes. This is in contrast to non-permafrost areas, which experience highest warming during summer and autumn, with winter being less prominent.

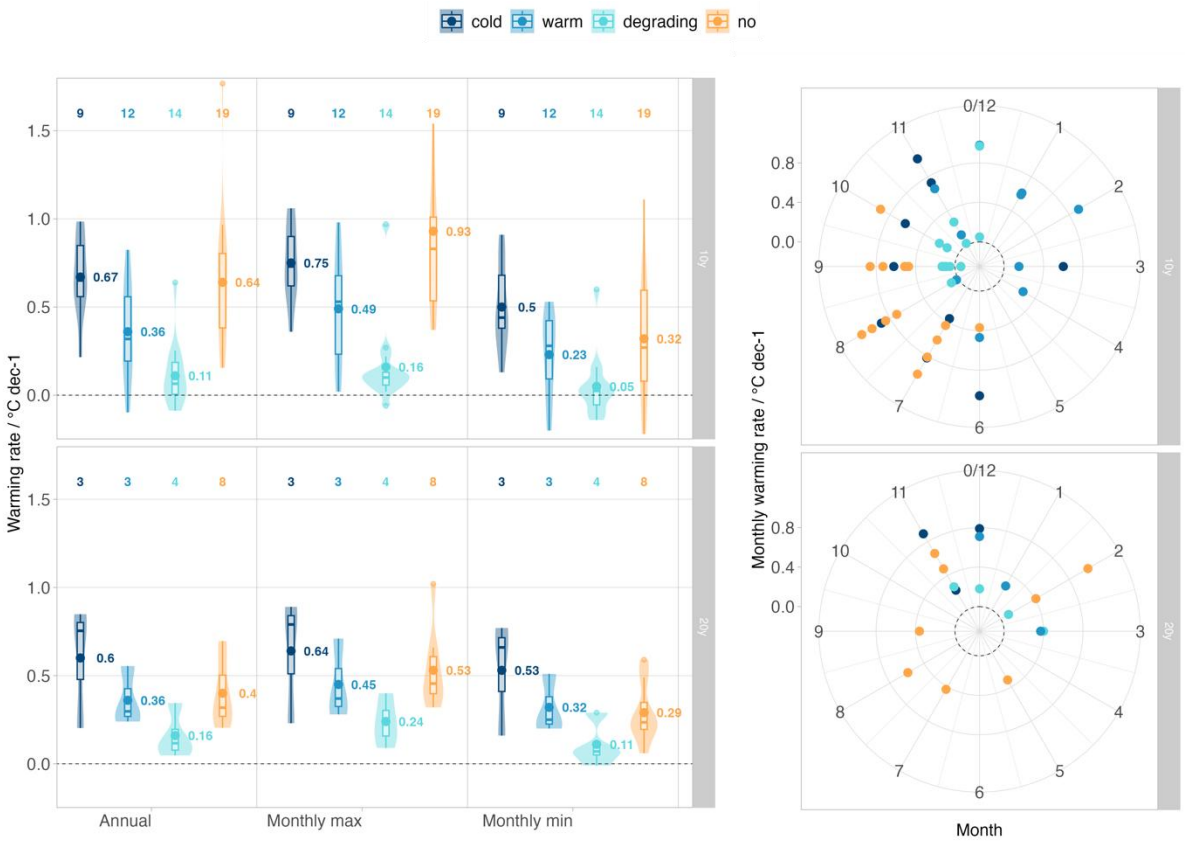

*Figure 7. Left panels: Annual (left) and monthly maximum (center) and minimum (right) warming rates at 10 m depth for the last available 10-year (top) and 20-year (bottom) periods. Permafrost classification (colors) and statistical distribution (boxplots) are given as in Figure 6. Right panels: Maximum monthly warming rate observed at 10 m depth for each individual time series over the last available 10- (top) and 20-year (bottom) periods plotted for the month in which they originate near the ground surface, considering the site-specific time delay necessary to reach 10 m depth. The highest value in the top plot amounts to 2.6 °C dec$^{-1}$ in July and is outside the plot area.*

## 3 Discussion

Permafrost in European mountains generally warmed since the start of thermal observations across all regions, depths and time periods considered in our analyses. Mountain permafrost in Europe is found in a large variety of landforms with different surface and subsurface characteristics, thermal conditions and topographic settings. Temperature changes in the permafrost are primarily driven by changes in air temperature [57], which are effective during periods with little or no snow, and all year round for locations where no thick snow cover develops during winter (e.g., near-vertical slopes or wind-blown ridges). Differences in the observed warming patterns depend in the first place on the amount of exchanged latent heat, which is related to the temperature range and ground ice content.

Warming rates for the latest available decade are generally higher than reported earlier for polar and mountain permafrost regions [3,4,6,8,55]. Most likely, this is partly a result of the considered sample, since earlier studies mainly considered time series obtained in warm and degrading permafrost in sedimentary landforms, for which measurements typically started earlier. Observations from cold high-elevation bedrock sites, where highest warming rates are observed, have only just reached lengths that enable the evaluation of their long-term changes. A fast temperature increase in near-vertical bedrock slopes, ridges and peaks can be accelerated by extreme Alpine topography, where heat transfer from the surrounding air can happen from various directions [58]. Highest warming rates in cold permafrost, instead, are in line with previous observations, based mainly on lowland polar permafrost sites [4].

In the decade 2013–2022, ground temperature change rates at a depth of 10 m in cold and no permafrost, as well as in ice-poor bedrock slopes, are in the range of 0.4–0.7 °C dec$^{-1}$. This is comparable to SAT change rates derived for the Alpine and Scandinavian regions [59] (Fig. 6). Atmospheric warming was comparatively homogeneous over the Alpine region and pronounced from 1980 onwards [60], which is when the first permafrost data became available. In the Scandinavian mountains, SAT warming over recent decades have not been systematically investigated but we derived values comparable to the European Alps (Fig. 6a, cf. section 4). In western Svalbard, 1981–2020 SAT warming rates between 1.0 °C and 1.2 °C dec$^{-1}$ were observed near the permafrost monitoring sites [61].

Change rates in ice-bearing and ice-rich ground at temperatures between ca. –2 and 0 °C are reduced due to the uptake of latent heat during phase change. Warming rates typically decrease towards the melting point and are significantly lower than those of SAT. Just below 0 °C, ground temperature in ice-rich terrain can remain stable for years, despite considerably changing air temperatures [4,8,11].

Conversely, however, small warming rates in warm and degrading permafrost do not imply the absence of changes in the permafrost. On the contrary: in ice-bearing ground, large changes in (un-)frozen water content take place in this temperature range, which can have critical impact on the geotechnical and hydrological characteristics of the ground. These changes cannot be recorded with temperature measurements as ice and water can co-exist at 0 °C. Complementing measurements, like repeated geoelectrical surveys, have to be used. Such techniques revealed considerable changes in unfrozen water content at many mountain permafrost sites in the Alps and Scandinavian mountains, pointing to a substantial and irreversible loss of ground ice [7,9,42,62–64]. After such permafrost degradation, ground temperature response can be abrupt, leading to very high warming rates. Indeed, the highest warming rate observed in this study is related to a sudden increase in ground temperatures after the ground ice degradation and corresponding cessation of latent heat effects [42] : at the Dovrefjell DB6 site, MAGT strongly increased after permafrost degraded completely in 2017. This is the lowest lying site among those in southern Scandinavia and exhibits a significant lag in response to SAT rise over the recent decades, mainly due to considerable ground ice content and typically late winter snow cover. Observed cooling rates are very small and occur at sites with ground temperatures close to the melting point, where annual variations in MAGT are in the order of magnitude of the measurement accuracy. Therefore, we do not consider these as an actual significant effect of cooling conditions.

Depending on the measurement depth, permafrost temperature series exhibit considerable intra- and interannual variations. This poses challenges in deriving robust warming rates when calculated over shorter time periods (e.g. a decade). Particularly, values obtained in the uppermost metres are influenced by exceptional warm or cold years and by natural variability [65]. We obtain the most robust warming rates at 20 m depth (i.e. below the DZAA) and for periods of two decades, albeit only few such time series are available. Changes in permafrost temperature at a depth of around 10 m reflect the systematic seasonal variations at the ground surface, but with a smaller amplitude and a phase lag, as higher-frequency near-surface signals are filtered out.

The results from the seasonal analyses are consistent with previously reported changes in SAT, radiation and snow cover, as well as with their influence on the permafrost thermal regime. For the last decade in particular, the higher summer and autumn SAT in Europe [59,66] seem to have been important contributors to permafrost warming. This is also in line with modelling of the sensitivity of permafrost to seasonal air temperature and precipitation anomalies [67]. It is noteworthy that recent summer and autumn SAT in Europe have seemingly increased due to the increase in surface solar radiation (C3S 2023) [68]. Highest annual surface solar radiation levels were, for example, observed during the warmest European summer 2022. Distribution and changes of mountain permafrost strongly depend on net radiation [69], which can for example result in a different thermal response at different slope expositions in high-elevation bedrock [11]. However, there are local to regional variations, and the response at individual sites is intricate. The aforementioned effects influence the various sites to varying degrees [70]

and contribute to understand the discrepancies in warming rates observed across various surface cover and expositions among our monitoring sites.

In addition to SAT and radiation, the timing of the winter snow cover must be considered, which can temporarily reduce or enhance a general warming pattern. Typically, an early snow cover conserves the summer heat in the ground, while a long-lasting snow cover insulates the ground from increasing air temperatures in spring or early summer, and vice-versa. For example, a temporary cooling of the permafrost down to more than 10 m despite higher air temperatures, was observed following the snow poor winters 2016 and 2017 in the European Alps [8,71]. Snow cover duration in the Alps has been decreasing even at the highest elevations, particularly due to an earlier snow melt in spring [72,73]. A longer snow free season in spring and early summer has the potential to amplify non-linear processes such as albedo feedbacks, and to accelerate permafrost warming by corresponding changes in the ground heat fluxes [70]. For the analysed 20-year period, near-surface warming was the most dominant in winter (Fig. 7), in agreement with long-term changes in SAT and snow cover. In Scandinavia, an increase in winter precipitation since 1961 was observed, resulting in greater snow accumulation in the highest mountains [74] and contributing to the permafrost warming in e.g. Norway [42]. In Svalbard, the highest SAT rates were observed during autumn and winter [61]. Here, monitoring sites are snow poor, making the late autumn and winter warming's impact on the permafrost strongest, as indicated in our seasonal analysis.

Permafrost observation sites are geographically unevenly distributed, with a bias towards more accessible locations or pre-existing research sites [12]. While mountain permafrost research was initiated in the 1970s with studies on prominent rock glacier landforms [46], permafrost in near-vertical rock has been in the focus of research after the 2003 summer heat wave. Several existing time series in bedrock slopes are still too short to be integrated into this study. Sites at higher elevations and with temperatures likely a few degrees lower than those available to date, are not yet available. Geographically, the eastern end of the Alpine Arc, the Pyrenees, and remote sites in Scandinavia and Svalbard, are still underrepresented. But above all, mountain permafrost observations remain rare outside of the comparatively accessible European mountains, with noticeable lacks of observations in the Rocky Mountains, the Central Asian Mountain ranges, the Himalaya and the Andes.

Maintaining measurement instruments in harsh environment over decades to acquire uninterrupted, robust and comparable records of permafrost temperature is very challenging. Standards for site selection and measurement protocols have only recently been discussed and elaborated [38,75]. Although the systematic organization and curation of the obtained data in national and international data centres has evolved in the past years, most of the time series included in this study are not secured in the long-term and only a part is centrally managed in (inter)national databases. Further, challenges of site maintenance are increasing with changing permafrost conditions at the observations sites and will likely increase further in the future. Problems related to the aging of instruments and their timely replacement must be solved, while instruments may become inaccessible due to field safety concerns. The urgent

need for international and national efforts for permafrost monitoring, data curation and sharing, as well as updated reports on changes, have just recently been highlighted by the World Meteorological Organization (2023) and in international political framework (Scientific statement on cryosphere of the Paris Call for Glaciers and Poles, 2023). Such monitoring is vital for assessing the impact of atmospheric warming on permafrost, as well as for improved model validation, for stakeholders, and for addressing the challenges posed by the degradation of permafrost in mountain areas.

# 4 Methods

## 4.1 Measurement of permafrost temperatures

Ground temperature time series for mountain permafrost are obtained in boreholes of around 10–100 m depth, which are drilled vertically in most cases, but also horizontally through crests or perpendicular to the surface in near-vertical bedrock slopes. Temperatures are obtained by automated continuous data logging at different depths with permanently installed multi sensor cables and recording intervals of 1–24h. Thermistors are the most often used sensors for permafrost temperature measurements. Temperature sensor strings are typically calibrated in an ice-water bath together with the logging system at 0 °C prior to installation in the borehole. The drilling and instrumentation of boreholes in harsh, cold environments with difficult access, and their long-term operation to obtain series over decades are technically and logistically challenging. For details on the measurement procedure see for example Noetzli et al. [38] or Streletskiy et al. [75].

Typical measurement accuracies reported for permafrost boreholes vary from about ±0.01 to ±0.25 °C, depending on the sensors and logging system [3,38,75]. Gaps in the time series may occur due to power failure or damage because of moisture intrusion, natural hazards (storm, lightning, avalanches, rock fall), or disruption by animals. Potential inconsistencies in the time series may result from changes in the measurement setup (such as replacement of sensor cables or loggers), moisture or water intrusion into the borehole, cables or sensors (particularly for sites with temperatures close to 0°C with higher unfrozen water contents), sensor or cable damage due to ground deformation or shearing, or sensor drift over time. Re-calibration of the system to assess the latter is often not possible as sensor cables can be stuck in the borehole, particularly in ice-rich deforming ground such as in rock glaciers [76]. Quality control of the data primarily relies on value-range and consistency checks, as well as plausibility assessment based on either duplicate and neighbouring sensors or on data from nearby stations. A single drifting sensor is detectable through its strong anomalous temporal trend, which is not observed for neighbouring sensors.

## 4.2 Data collection and processing

Permafrost temperature time series measured in boreholes in European mountain regions were collected from global, national and regional networks. Additional data that were not openly available in (inter)national data centres were retrieved from environmental agencies, research institutions and individual researchers. The criteria to include a time series in our analyses were: the borehole is located

in permafrost regions in mountain terrain, reaches a depth of 10 m, MAGT is at or below 0 °C for two consecutive years, and the time series covers at least one decade (i.e., starting in the year 2014 or earlier). For comparison to changes in non-permafrost terrain, we additionally considered time series from boreholes located in close vicinity of permafrost areas or where permafrost has recently degraded.

We collected daily time series, performed basic quality checks (cf. Section 4.1), and aggregated them to monthly and annual mean values. Due to the higher temporal variability of ground temperatures near the surface, we define depth-dependent criteria for data completeness, i.e. for daily fluctuations (above 2 m depth, 12 monthly mean values required to calculate an annual mean), seasonal fluctuations (2–17 m depth, 10 monthly values required) or very small intra-annual fluctuations close to or below the DZAA (>17 m depth, 4 monthly values required).

For the analyses of warming patterns, borehole sites were classified based on their location as well as their permafrost conditions, surface cover, and ground ice-content (cf. Table 1). For the latter, basic information is available from the drilling logs or from geophysical soundings. Based on the landform and geology of each site, four classes were distinguished: no ice (i.e., no permafrost), ice-poor (estimated ground ice content <10%, assumed for all bedrock sites), ice-bearing (considerable and varying ground ice, estimated about 10–100% for talus slopes or block fields), and ice-rich (ice supersaturation in rock glaciers). While surface cover and ground ice content were considered a constant site characteristic, permafrost classes were assigned for each analysed time period and depth (cf. section 4.3): cold permafrost with mean ground temperature of the period (MGTp) <–2°C (likely negligible effects of latent heat), warm permafrost with MGTp between –2 and below –0.5°C (small effects of latent heat depending on ground and freezing characteristics), and degrading permafrost with MGTp of –0.5°C or but with a maximum MAGT not higher than 0 °C (considerable effects of latent heat during phase change depending on ground ice content). In line with the definition of permafrost, we distinguished non-permafrost from degrading permafrost when the maximum MAGT during the period was >0°C. That is, time series that degraded during the considered period were classified as no permafrost (or degraded permafrost as in Fig. 4).

### 4.3 Calculation of permafrost warming rates

With increasing depth, the evolution of the permafrost thermal regime integrates temperature changes registered over a longer time period, over a larger surface area, and with increasing delay. In previous works, permafrost warming rates were often derived at the depth of zero annual amplitude DZAA [e.g., 3,4]. This depth is particularly important when relying on irregular and infrequent manual temperature readings [6,75,e.g., 77]. However, modern logging systems record quasi-continuous temperature time series allowing for seasonal fluctuations to be factored out. In addition, the DZAA varies with changing surface temperatures over longer time periods and some boreholes, e.g. in near-vertical slopes, do not reach this depth. To compile a data set including as many records as possible, we analysed warming rates at three key depths defined for climate related long-term permafrost observation: 5, 10, and 20 m depth (cf.

Streletskiy et al. 2022). At 5 m depth, ground temperatures closely follow surface temperature variations while at 10 m depth, they are only characterized by seasonal variations. These are no longer observed at 20 m depth, which is typically below the DZAA. Due to different sensor depths in the individual boreholes, the sensors closest to the key depths were selected and time series of permafrost temperatures assigned to three depth classes. Due to specific site characteristics or longer gaps for the closest sensor, a few boreholes needed manual adaptation of this assignment (e.g., to correct for differences in borehole depth to actual distance to the surface in steep terrain). Non-vertical boreholes completely piercing a crest (i.e., Zugspitze/DE and Gemsstock/CH) were considered as being two boreholes, one on each side.

We calculate warming rates for the three depth classes for each time series of MAGT using ordinary least squares (OLS) linear regression in the R-environment. We do this for the last available decadal and 20-year period (i.e., 2013–2022 and 2003–2022). To assess the robustness of the obtained values and to put it into perspective with the previous time periods, we additionally calculate warming rates for all available 10-year and 20-year time periods. Thus, we obtain a running warming rate for each borehole time series of MAGT for 1–3 depths classes and with an averaging window of 1 or 2 decades starting from the first available year. For a non-parameteric distribution of data, the Theil-Sen Slope (TSS) is often preferred over the OLS method as it is less sensitive to outliers. Comparing results by applying both methods, however, shows marginal differences. Exceptional cases are ice-bearing sites with a sudden increase in MAGT above 0 °C after the permafrost has degraded since latent heat effects cease to play a role (Dovrefjell BH6/NO). In such a case, the OLS method is preferred since such a temperature increase is not an outlier but rather an actual, relevant signal.

Following Biskaborn et al. [3], we considered the following data completeness criteria to calculate a warming rate for a given period: one MAGT value at the start of the period (±1 year), one at the end of the period (±1 year) and a minimum of 5 (one decade) or 10 MAGT values (two decades). It is important to note that while the number of MAGT values used for a linear regression is relatively small (n of 5–10 for 1 decade, n of 10–20 for 2 decades), these are not independent individual observations. We argue that the nature of the MAGT data allows for the application of linear regression on time series covering one decade. Indeed, each value comprises a compilation of daily observations spanning one year and short-term variations are filtered with increasing depth. In addition, due to slow thermal diffusion, ground temperatures at depth are the result of a signal emerging over a longer time span. Further, this approach has been widely applied to determine permafrost temperature warming rates [3,e.g., 4,7,8]. At several of the sites, more than one boreholes is located in close vicinity, but in different topographic settings or with differing site characteristics leading to different thermal regimes. We therefore refrained from calculating mean values per site before assessing change rates for the different categories.

To better understand the seasonal distribution of warming, we examined linear trends in monthly ground temperatures near the ground surface at approximately 0.2 m depth, at 5 m depth and at 10 m depth for the last available 10 and 20y periods (2013–2022 and 2003–2022). MAGT amplitudes near the surface

were also calculated. This happened at 5 m and 10 m depth. At 5 m depth some locations lacked measurements. At 10 m depth, nearly all locations had measurements and generally, the monthly ground temperature trends revealed a prominent annual cycle with noticeable differences between the months with the highest and lowest temperature trends. Consequently, the 10 m depth was selected for subsequent analyses. The maximum and minimum monthly warming rates were calculated, along with the corresponding months in which they occurred. To identify the month with the highest change rate near the ground surface, we analyzed the month with the maximum warming rate at 10 m depth and corrected for the corresponding phase lag in relation to the surface. To do so, the phase speed of the annual wave was computed by comparing the time difference between the average monthly maximum temperature at approximately 0.2 m and 10 m depth.

Time series of mean annual air temperature (MAAT) from weather stations located at or close to several of the actual permafrost boreholes were used to derive SAT change rates. We compiled data from three high elevation stations of MeteoSwiss (to avoid effects of local topography or valleys: Piz Corvatsch at 3294 m asl., Jungfraujoch at 3571 m asl. and Weissfluhjoch at 2691 m asl.), three MET Norway stations (Juvvasshøe, Fokstugu and Iskoras) and one UNIS station (Janssonhaugen, Svalbard). The sites are representative for the three main regions: the European Alps, Scandinavian mountains and Svalbard. In the absence of MAAT data at the beginning of three of the Scandinavian and Svalbard series (Juvvasshøe, Iskoras, and Janssonhaugen), the high-resolution Norwegian reanalysis named NORA3 [78] was employed to extend the datasets. For direct comparison with the original instrumental observations and to derive a value at the station locations, the NORA3 data series were adjusted by regression analysis ($R^2$ 0.95–0.97). To derive air temperature change rates we applied the OLS method as for permafrost time series, but for a time period of three decades (1993–2022) due to the higher interannual variability of air temperatures compared to the naturally filtered ground temperatures. As for permafrost temperature time series, the application of the TSS method led to negligible differences.

## References


1. Zemp, M. *et al.* Historically unprecedented global glacier decline in the early 21st century. *J. Glaciol.* **61**, 745-+ (2015).
2. Hugonnet, R. *et al.* Accelerated global glacier mass loss in the early twenty-first century. *Nature* **592**, 726–731 (2021).
3. Biskaborn, B. K. *et al.* Permafrost is warming at a global scale. *Nat. Commun.* **10**, 264 (2019).
4. Smith, S. L., O'Neill, H. B., Isaksen, K., Noetzli, J. & Romanovsky, V. E. The changing thermal state of permafrost. *Nat. Rev. Earth Environ.* **3**, 10–23 (2022).

5. Isaksen, K. *et al.* Advances in operational permafrost monitoring on Svalbard and in Norway. *Environ. Res. Lett.* **17**, 095012 (2022).
6. Romanovsky, V. E., Smith, S. L. & Christiansen, H. H. Permafrost thermal state in the polar Northern Hemisphere during the international polar year 2007-2009: a synthesis. *Permafr. Periglac. Process.* **21**, 106–116 (2010).
7. Etzelmüller, B. *et al.* Twenty years of European mountain permafrost dynamics—the PACE legacy. *Environ. Res. Lett.* **15**, 104070 (2020).
8. Haberkorn, A., Kenner, R., Noetzli, J. & Phillips, M. Changes in Ground Temperature and Dynamics in Mountain Permafrost in the Swiss Alps. *Front. Earth Sci.* **9**, 626686 (2021).
9. PERMOS. *Swiss Permafrost Bulletin 2022*. 23 (2023).
10. Zhao, L. *et al.* Changing climate and the permafrost environment on the Qinghai–Tibet (Xizang) plateau. *Permafr. Periglac. Process.* **31**, 396–405 (2020).
11. Magnin, F. *et al.* Main results of permafrost monitoring in the French Alps through the *PermaFrance* network over the period 2010–2022. *Permafr. Periglac. Process.* ppp.2209 (2023) doi:10.1002/ppp.2209.
12. Hock, R. *et al.* High mountain areas. in *IPCC Special Report on the Ocean and Cryosphere in a Changing Climate* 131–202 (2019).
13. Belward, A. *et al. The Global Observing System for Climate: Implementation Needs*. (2016).
14. Gruber, S. A Global View on Permafrost in Steep Bedrock. in *10th International Conference on Permafrost* 131–136 (2012).
15. Obu, J. *et al.* Northern Hemisphere permafrost map based on TTOP modelling for 2000–2016 at 1 km2 scale. *Earth-Sci. Rev.* **193**, 299–316 (2019).
16. Kenner, R., Noetzli, J., Hoelzle, M., Raetzo, H. & Phillips, M. Distinguishing ice-rich and ice-poor permafrost to map ground temperatures and ground ice occurrence in the Swiss Alps. *The Cryosphere* **13**, 1925–1941 (2019).
17. Deluigi, N., Lambiel, C. & Kanevski, M. Data-driven mapping of the potential mountain permafrost distribution. *Sci. Total Environ.* **590–591**, 370–380 (2017).
18. Gruber, S. & Haeberli, W. Mountain Permafrost. in *Biology Series* 33–44 (Springer, 2009).

19. Ravanel, L. & Deline, P. Climate influence on rockfalls in high-Alpine steep rockwalls: The north side of the Aiguilles de Chamonix (Mont Blanc massif) since the end of the 'Little Ice Age'. *The Holocene* **21**, 357–365 (2011).
20. Fischer, L., Purves, R. S., Huggel, C., Noetzli, J. & Haeberli, W. On the influence of topographic, geological and cryospheric factors on rock avalanches and rockfalls in high-mountain areas. *Nat. Hazards Earth Syst. Sci.* **12**, 241–254 (2012).
21. Huggel, C., Clague, J. J. & Korup, O. Is climate change responsible for changing landslide activity in high mountains? *Earth Surf. Process. Landf.* (2012) doi:10.1002/esp.2223.
22. Krautblatter, M., Funk, D. & Günzel, F. K. Why permafrost rocks become unstable: a rock-ice-mechanical model in time and space. *Earth Surf. Process. Landf.* **38**, 876–887 (2013).
23. Coe, J. A., Bessette-Kirton, E. K. & Geertsema, M. Increasing rock-avalanche size and mobility in Glacier Bay National Park and Preserve, Alaska detected from 1984 to 2016 Landsat imagery. *Landslides* **15**, 393–407 (2018).
24. Phillips, M. *et al.* Rock slope failure in a recently deglaciated permafrost rock wall at Piz Kesch (Eastern Swiss Alps), February 2014. *Earth Surf. Process. Landf.* 1–13 (2016) doi:10.1002/esp.3992.
25. Guglielmin, M., Ponti, S., Forte, E. & Cannone, N. Recent thermokarst evolution in the Italian Central Alps. *Permafr. Periglac. Process.* **32**, 299–317 (2021).
26. Walter, F. *et al.* Direct observations of a three million cubic meter rock-slope collapse with almost immediate initiation of ensuing debris flows. *Geomorphology* **351**, 106933 (2020).
27. Haeberli, W., Schaub, Y. & Huggel, C. Increasing risks related to landslides from degrading permafrost into new lakes in de-glaciating mountain ranges. *Geomorphology* **293**, 405–417 (2017).
28. Shugar, D. H. *et al.* A massive rock and ice avalanche caused the 2021 disaster at Chamoli, Indian Himalaya. *Science* **373**, 300–306 (2021).
29. Duvillard, P.-A., Ravanel, L., Marcer, M. & Schoeneich, P. Recent evolution of damage to infrastructure on permafrost in the French Alps. *Reg. Environ. Change* **19**, 1281–1293 (2019).
30. Cannone, N., Sgorbati, S. & Guglielmin, M. Unexpected impacts of climate change on alpine vegetation. *Front. Ecol. Environ.* **5**, 360–364 (2007).

31. Frey, B. *et al.* Microbial diversity in European alpine permafrost and active layers. *Fems Microbiol. Ecol.* **92**, (2016).
32. Jin, X.-Y. *et al.* Impacts of climate-induced permafrost degradation on vegetation: A review. *Adv. Clim. Change Res.* **12**, 29–47 (2021).
33. Ponti, S. A new simple topo-climatic model to predict surface displacement in paraglacial and periglacial mountains of the European Alps: The importance of ground heating index and floristic components as ecological indicators. *Ecol. Indic.* (2021).
34. Krainer, K. & Mostler, W. Hydrology of Active Rock Glaciers: Examples from the Austrian Alps. *Arct. Antarct. Alp. Res.* **34**, 142–149 (2002).
35. DeBeer, C. M., Wheater, H. S., Carey, S. K. & Chun, K. P. Recent climatic, cryospheric, and hydrological changes over the interior of western Canada: a review and synthesis. *Hydrol. Earth Syst. Sci.* **20**, 1573–1598 (2016).
36. Jin, X. *et al.* Impacts of Permafrost Degradation on Hydrology and Vegetation in the Source Area of the Yellow River on Northeastern Qinghai-Tibet Plateau, Southwest China. *Front. Earth Sci.* **10**, 845824 (2022).
37. Streletskiy, D. *et al.* Strategy and Implementation Plan for the Global Terrestrial Network for Permafrost (GTN-P) 2021-2024. (2021) doi:10.5281/ZENODO.6075468.
38. Noetzli, J. *et al.* Best Practice for Measuring Permafrost Temperature in Boreholes Based on the Experience in the Swiss Alps. *Front. Earth Sci.* **9**, 607875 (2021).
39. GCOS. *The 2022 GCOS Implementation Plan*. 86 https://library.wmo.int/viewer/58104/download?file=GCOS-244_2022_GCOS_Implementation_Plan.pdf&type=pdf&navigator=1 (2022).
40. Pogliotti, P., Cremonese, E. & Cella, U. M. D. Warming Permafrost in the Western Alps: A Further Evidence of Elevation Dependent Warming? *Rev. Géographie Alp.* (2023) doi:10.4000/rga.11784.
41. Isaksen, K. *et al.* Degrading Mountain Permafrost in Southern Norway: Spatial and Temporal Variability of Mean Ground Temperatures, 1999--2009. *Permafr. Periglac. Process.* **22**, 361–377 (2011).

42. Etzelmüller, B. *et al. Rapid Warming and Degradation of Mountain Permafrost in Norway and Iceland*. https://tc.copernicus.org/preprints/tc-2023-50/ (2023) doi:10.5194/tc-2023-50.
43. Barsch, D. Active rock glaciers as indicators for discontinuous alpine permafrost: an example from the Swiss Alps. in *Proceedings of the 3rd International Conference on Permafrost* vol. 1 349–353 (National Research Council of Canada, Edmonton, Alberta, Canada, 1978).
44. Haeberli, W. Untersuchungen zur Verbreitung von Permafrost zwischen Flüelapass und Piz Grialetsch (Graubünden). (ETH Zurich, Zurich, Switzerland, 1975).
45. Harris, S. A. & Brown, J. Plateau Mountain: a case study of alpine permafrost in the Canadian Rocky Mountains. in *Proceedings of the 3rd International Conference on Permafrost* vol. 1 386–391 (National Research Council of Canada, Edmonton, Alberta, Canada, 1978).
46. Haeberli, W. *et al.* Mountain permafrost: development and challenges of a young research field. *J. Glaciol.* **56**, 1043–1058 (2010).
47. Haeberli, W. *et al.* Core drilling through rock glacier-permafrost. in 937–942 (Tapir Publishers, Trondheim, Trondheim, Norway, 1988).
48. Vonder Mühll, D. & Haeberli, W. Thermal characteristics of the permafrost within an active rock glacier (Murtèl/Corvatsch, Grisons, Swiss Alps). *J. Glaciol.* **36**, 151–158 (1990).
49. Harris, C., Haeberli, W., Vonder Mühll, D. & King, L. Permafrost monitoring in the high mountains of Europe: the PACE Project in its global context. *Permafr. Periglac. Process.* **12**, 3–11 (2001).
50. Haeberli, W. *et al.* Monitoring the long-term evolution of mountain permafrost in the Swiss Alps. in *6th International Permafrost Conference* 214–219 (Beijing, China, 1993).
51. Vonder Mühll, D., Noetzli, J. & Roer, I. PERMOS - a comprehensive monitoring network of mountain permafrost in the Swiss Alps. in *Proceedings* 1869–1874 (Fairbanks, US, 2008).
52. Schoeneich, P., Bodin, X., Krysiecki, J.-M., Deline, P. & Ravanel, L. *Permafrost in France*. 68 (2010).
53. Kellerer-Pirklbauer, A., Kaufmann, V., Avian, M. & Lieb, G. K. One decade of comprehensive permafrost monitoring in Austria by the Graz Permafrost Monitoring Network: A status report. in (2017).

54. Farbrot, H. *et al.* Air and Ground Temperature Variations Observed along Elevation and Continentality Gradients in Southern Norway. *Permafr. Periglac. Process.* **22**, 343–360 (2011).
55. Christiansen, H. H. *et al.* The thermal state of permafrost in the nordic area during the international polar year 2007–2009. *Permafr. Periglac. Process.* **21**, 156–181 (2010).
56. Cremonese, E. *et al.* Brief Communication: 'An inventory of permafrost evidence for the European Alps'. *The Cryosphere* **5**, 651–657 (2011).
57. Kenner, R., Noetzli, J., Bazargan, M. & Scherrer, S. C. Response of alpine ground temperatures to a rising atmospheric 0 °C isotherm in the period 1955–2021. *Sci. Total Environ.* **924**, 171446 (2024).
58. Noetzli, J. & Gruber, S. Transient thermal effects in Alpine permafrost. *The Cryosphere* **3**, 85–99 (2009).
59. Simmons, A. J. Trends in the tropospheric general circulation from 1979 to 2022. *Weather Clim. Dyn.* **3**, 777–809 (2022).
60. Auer, I. *et al.* HISTALP—historical instrumental climatological surface time series of the Greater Alpine Region. *Int. J. Climatol.* **27**, 17–46 (2007).
61. Isaksen, K. *et al.* Exceptional warming over the Barents area. *Sci. Rep.* **12**, 9371 (2022).
62. Mollaret, C. *et al.* Mountain permafrost degradation documented through a network of permanent electrical resistivity tomography sites. *The Cryosphere* **13**, 2557–2578 (2019).
63. Pogliotti, P. *et al.* Warming permafrost and active layer variability at Cime Bianche, Western European Alps. *Cryosphere* **9**, 647–661 (2015).
64. Hilbich, C. *et al.* Monitoring mountain permafrost evolution using electrical resistivity tomography: A 7-year study of seasonal, annual, and long-term variations at Schilthorn, Swiss Alps. *J. Geophys. Res.* **113**, F01S90 (2008).
65. von Storch, H. & Zwiers, F. W. *Statistical Analysis in Climate Research*. (1999).
66. Rottler, E., Kormann, C., Francke, T. & Bronstert, A. Elevation-dependent warming in the Swiss Alps 1981–2017: Features, forcings and feedbacks. *Int. J. Climatol.* **39**, 2556–2568 (2019).
67. Marmy, A., Salzmann, N., Scherler, M. & Hauck, C. Permafrost model sensitivity to seasonal climatic changes and extreme events in mountainous regions. *Environ. Res. Lett.* **8**, 035048 (2013).

68. Philipona, R., Marty, C., Duerr, B. & Ohmura, A. Rising solar and thermal greenhouse radiation drive rapid warming over continents. *Meteorol. Z.* **32**, 5–14 (2023).
69. Hoelzle, M., Mittaz, C., Etzelmüller, B. & Haeberli, W. Surface energy fluxes and distribution models of permafrost in European mountain areas: an overview of current developments. *Permafr. Periglac. Process.* **12**, 53–68 (2001).
70. Hoelzle, M. *et al.* Long-term energy balance measurements at three different mountain permafrost sites in the Swiss Alps. *Earth Syst. Sci. Data* **14**, 1531–1547 (2022).
71. PERMOS. *Permafrost in Switzerland 2014/2015 to 2017/2018*. 104 (2019).
72. Kotlarski, S. *et al.* 21st Century alpine climate change. *Clim. Dyn.* **60**, 65–86 (2023).
73. Marty, C., Tilg, A.-M. & Jonas, T. Recent Evidence of Large-Scale Receding Snow Water Equivalents in the European Alps. *J. Hydrometeorol.* **18**, 1021–1031 (2017).
74. Dyrrdal, A. V., Saloranta, T., Skaugen, T. & Stranden, H. B. Changes in snow depth in Norway during the period 1961–2010. *Hydrol. Res.* **44**, 169–179 (2013).
75. Streletskiy, D. *et al.* Measurement Recommendations and Guidelines for the Global Terrestrial Network for Permafrost (GTN-P). (2022) doi:10.5281/ZENODO.5973079.
76. Luethi, R. & Phillips, M. Challenges and solutions for long-term permafrost borehole temperature monitoring and data interpretation. *Geogr. Helvetica* **71**, 121–131 (2016).
77. Burgess, M. M., Smith, S. L., Brown, J., Romanovsky, V. E. & Hinkel, K. The Global Terrestrial Network for Permafrost (GTNet-P): permafrost monitoring contributing to global climate observations. *Geol. Surv. Can.* (2000).
78. Haakenstad, H. & Breivik, Ø. NORA3. Part II: Precipitation and Temperature Statistics in Complex Terrain Modeled with a Nonhydrostatic Model. *J. Appl. Meteorol. Climatol.* **61**, 1549–1572 (2022).

## Data availability

The data generated during and analysed during the current study are available from the corresponding author on reasonable request. Annual mean permafrost temperature values for many of the time series

analysed are available in the GTN-P data base. Data from Switzerland are openly available at https://doi.org/10.13093/10.13093/permos-2023-01.

To be discussed if we should publish a DOI with the data set used in this study (monthly and annual mean ground temperatures at key depths) to make the data openly available.

## Code availability

All analyses were performed in R, version 4.3.2. All scripts can be obtained from the corresponding author upon reasonable request.


## Acknowledgements

Long measurement series such as those used in this study have been collected over a decade or more by a large number of people and institutions as part of regional and national measurement networks as well as research and monitoring projects. This long-term commitment and continuous work, including all the support for field work and instrument maintenance, is greatly acknowledged and cannot be overestimated.

Permafrost data acquistion in Switzerland is organized by the Swiss Permafrost Monitoring Network PERMOS and financially supported by MeteoSwiss, in the framework of GCOS Switzerland, the Federal Office for the Environment FOEN and the Swiss Academy of Sciences SCNAT. The data collection at Stelvio is supported by the Progetti di Ricerca di Rilevante Interesse Nazionale - PRIN 2015, grant number 2015N8F555 and the Stelvio National Park.

=> please provide your information that has to go in there!


## Author contributions

The study was initiated by JN and KI during discussion on 20year results of the European PACE transect and as an in-depth study of mountain permafrost following the global assessment by Biskaborn et al. 2019. JN led the data collection, processing, and analyses and writing of the manuscript with strong support from KI, who is the principal co-author and performed the seasonal analyses. All authors are current principal investigators of at least one borehole site and contributed with data collection and expert knowledge on instrumentation and site characteristics required for the interpretation of the results. All authors also contributed to the manuscript with feedback and discussions on earlier versions.

## Competing interests

The authors declare no competing interests.

## Figure legends

## Tables

## Supplementary information

- Overview plots showing the monthly mean and MAGT time series for the three depths for each borehole (i.e. the basic data input)
- Overview plot showing the running decadal warming rates for the three depths for each borehole
- Plots with classified warming rates for all depth classes and time periods (10 m and 20 m, 10y and 20 y)